Heliyon 10 (2024) e36983

Contents lists available at ScienceDirect

Heliyon

journal homepage: www.cell.com/heliyon

Research article

# Investigation on reconstruction of internal heat source in biological tissue based on multi-island genetic algorithm

Fuli Ye [a], Diwen Shi [a], Cheng Xu [a], Kaiyang Li [b], Minyue Lin [a], Guilian Shi [a,b,*]

[a] School of Biomedical Engineering and Imaging, Xianning Medical College, Hubei University of Science and Technology, Xianning, 437100, China
[b] School of Physics and Technology, Wuhan University, Wuhan, 430072, China

ARTICLE INFO

*Keywords:*
Multi-island genetic algorithm (MIGA)
Objective function
Reconstruction
Internal heat source
3D temperature field

ABSTRACT

With the rapid development of engineering thermophysics, researches on human biological heat transfer phenomena has gradually shifted from qualitative to quantitative. It is a typical inverse problem of heat conduction that deriving the distribution of internal heat sources from the temperature distribution on the body surface. Differing from traditional numerical methods for solving heat conduction, this paper transforms such an inverse problem of bio-heat transfer into a direct one, thereby avoiding complex boundary conditions and regularization processes. To noninvasively reconstruct the internal heat source and its corresponding 3D temperature field in biological tissue, the multi-island genetic algorithm (MIGA) is used in the simulation module, where the position P$(x, y, z)$ of point heat source in biological tissue and its corresponding temperature $T$ are set as the optimization variables. Under a certain optimized sample, one can obtain the simulated temperature distributing on the surface of the module, then subtract the simulated temperature from the measured temperature of the same surface which was measured using a thermal infrared imager. If the absolute value of the difference is smaller, it indicates that the current sample is closer to the true location and temperature of the heat source. When the values of optimization variables are determined, the corresponding 3D temperature field is also confirmed. The simulation results show the experimental and simulation temperature values of 15.5Ω resistor are 60.75°C and 62.15 °C respectively, with the error of 2.31 %, and those of 30.5Ω resistor are 84.40 °C and 86.33°C respectively, with the error of 2.29 %. The simulated positions are very approximate with those of the real experimental module. The method presented in this paper has enormous potential and promising prospects in clinical research and application, such as tumor hyperthermia, disease thermal diagnosis technology, etc.

## 1. Introduction

The noninvasive reconstruction of 3D temperature field in biological tissue is very valuable for the further development of biomedical engineering bioengineering field [1]. It is a typical heat conduction inverse problem that how the heat sources and the interior temperature field distribution are deduced through the surface temperature of living body [2–5]. The equation set formed for describing this kind of heat conduction inverse problems are often ill-posed, which doesn't mean they are unsolvable, but the solving

* Corresponding author. School of Biomedical Engineering and Imaging, Xianning Medical College, Hubei University of Science and Technology, Xianning, 437100, China.
*E-mail address:* glshi@whu.edu.cn (G. Shi).

https://doi.org/10.1016/j.heliyon.2024.e36983
Received 6 April 2024; Received in revised form 21 August 2024; Accepted 26 August 2024
Available online 27 August 2024

process is very cumbersome [6,7]. The traditional analytic methods can be hardly used in solving or analyzing the ill-posed problems. Even if the analytic methods are stiffly adopted, the solutions perhaps have no any realistic significance because of the great distance between the theoretical values and the real ones [8]. So the ill-posed problems often need a processing of regularization to make the obtained solutions more approximate to the real status [9–11]. Nowadays, the numerical methods such as boundary element method (BEM), finite element method (FEM), and finite difference method (FDM) are commonly used in the modeling and simulation of bio-heat conduction inverse problems [8,12–14]. However, these methods are very strict with geometric profile of the simulation object, and need heavy computation [15–17]. In some researches, the decentralized fuzzy inference method (DFIM) is applied to reconstruct the internal temperature of the biological tissue during laser-induced thermal therapy, and the reconstruction results demonstrate that the DFIM can accurately reconstruct the internal temperature distribution of the tissue [18–22]. However, the reconstruction process is quite cumbersome and the efficiency needs further improvement. For these reasons, the numerical methods are not suitable for the modeling and simulation of bio-heat conduction reverse problems on account of the complexity of biological tissue and organs, and also face great difficulties in the clinical application [23–26].

Based on optimization platform of software ISIGHT, a novel method of acquiring the distribution information of heat source and the 3D temperature field adopting multi-island genetic algorithm (MIGA) is presented in this paper. Different heat sources are corresponding to different temperature field, and there exists an only mapping between them. Based on the basic heat conduction theory mentioned above, the position $P(x,y,z)$ and its corresponding temperature $T$ of point heat source in biological tissue are supposed as the optimization variables in this research. Due to the excellent global search performance of MIGA, the process of searching for the optimal values are accelerated efficiently. After determining the position and temperature of the heat source, its corresponding 3D temperature field is also determined accordingly. On account of the method and the optimization model presented in this paper, a heat-conduction reverse problem is transformed to be a direct one, which greatly reduces the complexity in solving such inverse heat conduction problems. The work in this paper possesses a significant and practical meaning in the clinical field such as tumor hyperthermia, disease thermal diagnosis technology, etc.

## 2. MIGA and establishment of objective function

### 2.1. Basic theory and operational steps of MIGA

In the field of biological heat transfer, the genetic algorithm has been applied to identify nonlinear parameters such as thermal conductivity and blood perfusion rate of biological tissues, providing a reliable methodological basis for identifying nonlinear parameters in control engineering. The traditional genetic algorithm (GA) is actually single population, which makes the optimization prone to mature prematurely and difficult to obtain optimal values. Compared to the shortcomings of traditional GA such as premature convergence, MIGA has made some improvements:①Introduce multiple islands (population tribes) for simultaneous optimization search, and assign different control parameters to different populations; ②Connect different populations through immigration operators; ③The essence population is formed by preserving the best individuals in each evolutionary generation of various populations through manual selection operators, which is used as the basis for judging the convergence of the algorithm. In this study, the location $P(x,y,z)$ and temperature $T$ of the heat source were set as optimization variables, which belongs to multi-objective optimization

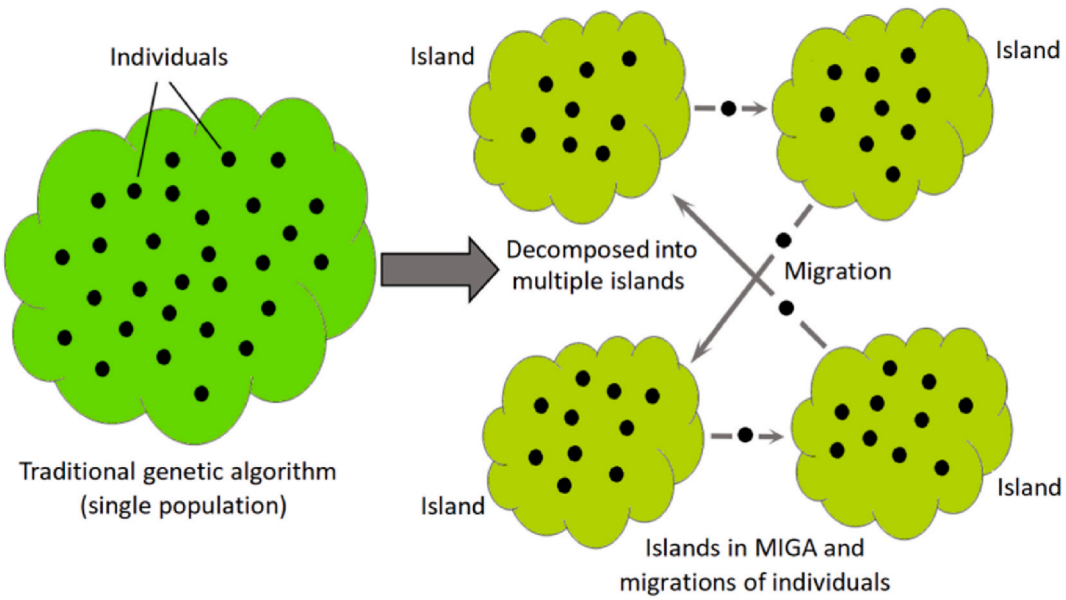


**Fig. 1.** The creating principle of island in MIGA.

problems. As a pseudo parallel algorithm, the MIGA can efficiently search for the global optimal solution in the optimization domain, avoiding premature convergence and improving convergence speed. The MIGA increases sample diversity with only a slight increase in computational complexity, in which the number of populations does not increase, only the population is decomposed into several islands, and traditional genetic calculations are performed on each island with a certain probability of gene crossover between islands. The main intention is to increase the algorithm's multimodal search ability and avoid falling into local optima. Therefore, the MIGA instead of GA were chosen to complete this research.

The MIGA, being derived from traditional genetic algorithm, first decomposes the entire evolutionary population into several subpopulations (also known as "islands"), and then performs corresponding genetic operations [27,28]. Shown as Fig. 1, for each subpopulation obtained after decomposition, genetic operations, including selection, crossover and variation, are performed with independent criteria. The algorithm adopts the roulette method in the selection mechanism, in which the best individual is copied from the previous generation to the next generation using an excellent individual retention strategy [29,30]. In order to ensure the diversity of the population and suppress premature convergence of the algorithm, the MIGA selects certain individuals for inter-island migration, which means individuals can be transferred from one island to another periodically and randomly, and the inter-island migration coefficient determines the number of generations that need intergenerational migration. Therefore, compared to traditional genetic algorithms, the MIGA has better optimization efficiency and global search ability [31–35].

The MIGA repeatedly utilizes the operators and selection principles of genetic algorithms to reproduce and evolve generation by generation, thereby making the population more adaptable to the environment. The operation steps of MIGA are as follows [32, 36–39]:

(1) Initialize the population, and decompose the single population into multiple islands.
(2) Calculate the fitness value of each individual in the islands, and select individuals who will enter the next generation based on a certain rule determined by individual fitness values.
(3) Perform crossover operation based on probability $P_c$.
(4) Perform mutation operation based on probability $P_m$.
(5) Perform inter-island migration operation based on probability $P_{mig}$.
(6) If a certain stopping condition is not met, then proceed to step (2), otherwise proceed to step (9).
(7) Identify the individual with the optimal target value and output it as the optimal solution.

MIGA is a pseudo parallel optimization algorithm, which increases the diversity of gene duplication due to a certain probability of inter-island migration among individuals [40,41]. Therefore, compared with traditional genetic algorithm, it has advantages such as high computational efficiency and avoiding premature convergence.

### 2.2. Establishment of objective function

In the optimization model, the position *P(x, y, z)* of internal point heat source and its corresponding temperature *t* are set as the optimal variables. All possible positions in the model and their temperature values form the whole sample space. According to the basic theory of heat conduction, each sample corresponds to a certain surface temperature distribution, which is the basis for constructing the objective function. Under a certain optimized sample, one can obtain the simulated temperature distributing on the surface of the module, then subtract the simulated temperature from the measured temperature of the same surface which was measured using a thermal infrared imager. If the absolute value of the difference is smaller, it indicates that the current sample is closer to the true location and temperature of the heat source. When the values of optimization variables are determined, the corresponding 3D temperature field is also confirmed. The objective function is expressed as follow:

$$f_{\min}(x, y, z, t) = \sum |T_n - T_{En}| \tag{1}$$

In Eq. (1), $T_n$ and $T_{En}$ are the simulated temperature and the experimental temperature respectively of a same point on surface, $n$ denotes the number of points. By the iterative calculation method shown as Eq. (1), one can determined the optimal position and its corresponding temperature value of point heat source, and then the distribution information of 3D temperature field in biological tissue can be acquired accordingly. It is typical heat conduction reverse problem how the internal temperature field distribution and the heat source distribution are derived from the surface temperature. This paper presents a optimal model that can exactly transform the reverse problem to a direction one, avoiding the tedious processing procedure of traditional numerical method such as regularization and boundary condition processing. In most practical cases, the surface temperature is often taken as boundary condition (belongs to the Dirichlet boundary condition), which means one has to firstly obtain all the surface temperature data in traditional numerical methods. The processing is complex or even unacquirable as far as the real living organism is concerned. The optimization method and model presents in this paper overcomes the difficulties above successfully, and just needs limited surface temperature data which can be easily obtained with thermal infrared imager.

In this research, a novel method of establishing objective function is proposed in the optimization model to reduce the computation of searching for the optimal solution during the optimization process. In the infrared thermal image of experimental module, two straight lines that intersect vertically are set, and then some equidistant points are set on the lines (the number of points can be reasonable set according to the actual size of module). One can extract the temperature values of these points, and subtract them with the simulated temperature values of the corresponding points under a certain sample (a position of point heat source and its corre-

sponding temperature in space of samples), then acquire the sum of absolute value. This method is not only simple and practicable, but also avoiding the complex establishing process of objective function without affecting the precision of algorithm, and the optimization speed is promoted greatly. In regard to the analysis of heat source distribution and temperature field distribution, such a method has a high theoretical and practical value. So, Eq. (1) can be modified as follow:

$$f_{\min}(x,y,z,t) = \sum |T_{1n} - T_{E1n}| + \sum |T_{2n} - T_{E2n}| \tag{2}$$

Where $T_{1n}$ and $T_{2n}$ respectively denote the simulated temperature values of equidistant points chosen on the two orthogonal straight lines which are set on a certain surface of simulation model, $T_{E1n}$ and $T_{E2n}$ respectively denote the experimental temperature values of the chosen equidistant points on two orthogonal straight lines that are set on the experiment model. The lines and the points on the experiment model are perfectly mapping to those on the simulated model.

### 2.3. Reconstruction of 3D temperature field

Eq. (2) is taken as the objective function to perform the iterative computations. When the objective value $f_{\min}$ reaches to the minimum, the current sample (including the position of heat source and the corresponding temperature value) is just the optimal results. After determining the position and temperature of the heat source, its corresponding 3D temperature field in biological tissue is also determined accordingly. By such a method, a bio-heat conduction reverse problem is transformed to be a direct one. The finite element analysis software ANSYS and the typical Pennes bio-heat conduction model are adopted in our simulation. ANSYS is a large finite element analysis software which contains three typical heat conduction modes, and can perform thermal simulation and analysis under various complex circumstance. It is commonly recognized that Pennes bio-heat conduction equation is the best model for the analysis of bio-heat, which can be expressed as follow [42]:

$$\rho c \frac{\partial T}{\partial t} = \nabla(k \cdot \nabla T) + w_b \rho_b c_b (T_b - T) + Q_m \tag{3}$$

In Eq. (3), T (*x, y, z*) is the distribution function of internal temperature field, ρand c denote the density (Kg/m$^3$) and the thermal capacitivity (J/Kg·°C) of biological tissue respectively, $w_b$, $\rho_b$, $c_b$, and $T_b$ denote the blood perfusion rate (ml/s·ml$^{-1}$), blood density (Kg/m$^3$), blood thermal capacitivity (J/Kg·°C) and blood temperature (°C) respectively, and $Q_m$ is the metabolic heat (W/m$^3$). In our research, an infrared thermal imager was adopted to obtain the surface temperature of the biological tissue model, which was used to invert and deduce the position and temperature of the internal heat source. In the simulation model of this paper, the surface temperature obtained with the infrared thermal imager belongs to the Dirichlet boundary condition.

## 3. Experiment and data processing

### 3.1. Experimental material

The pork adipose tissue, whose density is 827 kg/m$^3$ and thermal conductivity is 0.1265 W/(m·K), is adopted in the experiment of bio-heat conduction. The size of pork adipose tissue is 7.5 cm × 2.4cm × 3.0 cm, two resistors (15.5Ω and 30.5Ω) are adopted as the internally installed heat sources, and the diameter of 4 wires is 0.5 mm. The temperature measuring tool of model surface is non-refrigerated focal plane infrared thermal imager whose temperature resolution is 0.05 °C, pix is 640 × 480, and focusing range is 0.5m ~ ∞. The high precision digital point-thermometer JM222, whose probe can reach to the very position of pork adipose tissue model where the resistors are placed, is adopted to detect the temperature of heat source.

### 3.2. Experimental process

The pork adipose tissue was incised to a cuboid form, taking the bottom rear corner on the right side of the pork adipose module as the origin to establish rectangular coordinate. So, according to the measurement of the pork adipose tissue, the length of the cuboid in *x* direction was 7.5 cm, the height in *y* direction was 2.4 cm, and the width in *z* direction was 3.0 cm (Shown as Fig. 2). Using a slim knife,

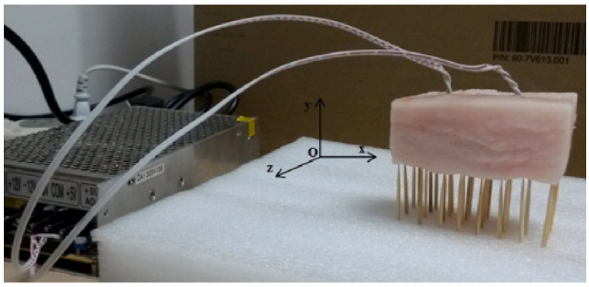


**Fig. 2.** Connection of pork adipose tissue and its support.

two incisions were made on the upper surface($y = 2.4$ cm) of the cuboid. The specific coordinates of the deepest point of one incision were $x = 2.5$ cm, $y = 1.7$ cm, $z = 1.6$ cm, meaning the depth of this incision was 0.7 cm, and those of the other incision were $x = 5.6$ cm, $y = 1.5$ cm, $z = 1.4$ cm, meaning the depth was 0.9 cm. A resistor(30.5Ω) was inserted into the adipose tissue module from the incision whose depth was 0.7 cm, reaching to deepest point; Another resistor(15.5 Ω) was inserted into the adipose tissue module from the incision whose depth was 0.9 cm, reaching to the deepest point. Two resistors were connected with a 5 V power supply. In order to ensure the six faces of adipose tissue module to be free for heat conduction and keep the shape as non-deforming as possible, some wooden toothpicks were adopted and aligned to be an array for supporting the adipose tissue module. When the two resistors were powered on, they began to generate heat and transferred it to the surface of the adipose tissue module. The surface temperature was detected using a infrared imager which was connected with a PC machine. When the heat conduction reached equilibrium, an infrared thermal image of the surface of the adipose tissue module at z = 3.0 cm was taken, in which the temperature data were extracted as fitness comparison data for optimizing iterative calculations. Meanwhile, the probe of digital point-thermometer was plugged to the position where the resistor located through the incision in the adipose tissue module, and the actual temperature value of heat source could be acquired. Based on the principle of fluid mechanics, when the airflow velocity $V \leq 0.15$ m/s and the environment temperature is 18~20 °C, the heat conduction of object surface in air belongs to laminar natural convection. Therefore, in the experiment procedure, the environment temperature was controlled at 19.4 °C, the windows and doors was kept close. In such circumstances, the laminar natural convection was set as 3.368 $W/m^2 \cdot K$ [43].

### 3.3. Experimental data and processing

A specialized temperature data processing software of infrared detector was adopted to extract the temperature values of 15 points which were distributed on two orthogonal straight lines on the surface z = 3.0 cm of adipose tissue module (Shown as Fig. 3). The specific position of two straight lines were ① $y = 1.7$ cm, $z = 3.0$ cm and ② $x = 5.0$ cm, $z = 3.0$ cm, respectively. Ten equidistant points were set on line ① and five equidistant points were set on line ②. The coordinate values of these 15 points and their corresponding temperature were given in Table 1. From theoretical aspect, the more points and wider the range selected from the surface of an infrared thermogram, the more accurate the simulation results will be. However, this will greatly increase the computational complexity of optimization iterations, thereby seriously reducing the efficiency of the algorithm. Therefore, a limited number of points are selected on the surface of the infrared thermogram in a certain way, which not only need to reflect the temperature distribution characteristics of the object surface, but also not have too many points that affect the efficiency of optimization. In this paper, two perpendicular lines were set on the infrared thermogram, which needed to pass through the highest temperature point of the thermogram. The 15 points selected on the straight lines basically spanned the most distinctive areas of the heatmap, which meant that temperature distribution characteristic of surface could be reflected via the 15 equidistant points. So, this method of selecting points not only ensured the speed of algorithm iteration calculation, but also guaranteed the accuracy of optimization results. The temperature values of two resistors at their middle position, measured with a point-thermometer, were 60.75 °C and 84.40 °C respectively. In fact, when the temperature of two resistors reached to a relatively high value, the adipose tissue around the resistors melted in a very small scale, which exerted some influence on the surface temperature distribution of experimental model. However, compared with the whole adipose tissue module, the proportion of melted adipose tissue was very small, which meant errors caused by the melted adipose tissue could be ignored. In practical procedure, the melted adipose tissue was regarded as a part of the heat source.

## 4. Simulation procedure and results

### 4.1. Establishment of ANSYS parameterized model

The heat conduction model of pork adipose tissue module was established with ANSYS parametric design language (APDL), which is the precondition that the ISIGHT automatically calls ANSYS and implements optimization procedure for acquiring the optimal heat source position and corresponding temperature distribution. APDL is a kind of scripting language affiliated to ANSYS itself. As a powerful tool and method, this language makes the application software ANSYS more convenient and perfect, and can automatically implement the finite element analysis [44]. Using APDL, the setting of parameters and the building of simulation model can be accomplished automatically, and also different analysis type can be chosen freely according to the need. Here, the size of simulation

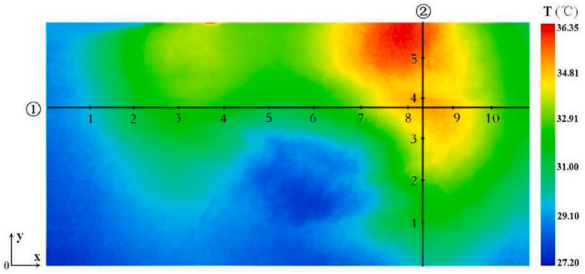


**Fig. 3.** Two straight lines and equidistant points acquired from the surface $z = 3.0$ cm of pork adipose tissue module.

**Table 1**
Coordinate values of 15 equidistant points from surface $z = 3.0$ cm of the pork adipose tissue module and their corresponding temperature values.

| Equidistant Points | Straight Line ① | | | Straight Line ② | | |
|---|---|---|---|---|---|---|
| | $x$/cm | $y$/cm | T/°C | $x$/cm | $y$/cm | T/°C |
| 1 | 0.68 | 1.70 | 29.82 | 5.00 | 0.40 | 29.24 |
| 2 | 1.36 | 1.70 | 31.98 | 5.00 | 0.80 | 30.28 |
| 3 | 2.05 | 1.70 | 33.06 | 5.00 | 1.20 | 31.95 |
| 4 | 2.73 | 1.70 | 33.22 | 5.00 | 1.60 | 34.02 |
| 5 | 3.41 | 1.70 | 32.75 | 5.00 | 2.00 | 35.65 |
| 6 | 4.09 | 1.70 | 31.79 | – | – | – |
| 7 | 4.77 | 1.70 | 33.55 | – | – | – |
| 8 | 5.45 | 1.70 | 34.75 | – | – | – |
| 9 | 6.14 | 1.70 | 34.21 | – | – | – |
| 10 | 6.82 | 1.70 | 33.02 | – | – | – |

model was set as $x = 7.5$ cm, $y = 2.4$ cm, $z = 3.0$ cm, the density was set as 827 kg/m$^3$ and the thermal conductivity was 0.1265 W/(m·K). The environment temperature was set as 19.4 °C, and the surface convective heat transfer coefficient was 3.368 W/m$^2$·K.

### 4.2. Simulation procedure and results

ISIGHT is a multidisciplinary optimization design platform, and commonly used in the engineering design field at present. It is developed out by Engineous Software Company of America based on Unix platform and Windows NT [43]. This software organically integrates design exploration technologies, reasoning technologies and digital technologies, and the functions are greatly expanded after the comprehensive exploitation. ISIGHT can also integrate multi-domain simulation code and afford corresponding intelligent support, realizing the evaluation and study to different design alternatives [44]. Such a process can greatly shorten the period of product design and promote the work efficiency [45,46]. The ISIGHT simulation procedure of reconstruction about the 3D temperature field was shown as Fig. 4.

In Fig. 4, the left dot denoted the beginning of computational process and the right one denoted the end computational process. The data transmission among the three data processing module was unidirectional. First, The module "MIGA Optimization" output the initialized variables to the module "ANSYS pork-fat 2-heatpoint". Then the module "ANSYS pork-fat 2-heatpoint" substituted the variables into the FEM model and worked out the result under a certain individual sample. The result was transmitted to the module "Objective Calculator"in which the calculation program of objective function was stored, and the module "Objective Calculator" could automatically work out the objective function value of each individual sample. Finally, as the evaluation basis of corresponding individual sample, this value was transmitted to the optimization module "MIGA Optimization" and the optimization module determined whether the replacement of a new sample was necessary according to the optimal settings such as the number of iterations, the setting of minimum value of objective function. In order to reduce the calculated amount and promote the optimization efficiency, a suitable objective function was established in the module "Objective Calculator". The calculation of objective value need combine the temperature data of 15 equidistant points on two straight lines which were set on the thermal image. The objective function in the "Objective Calculator" module was shown as Eq. (4).

$$\begin{aligned} f_{\min} = |T_{11} - 29.82| + |T_{12} - 31.98| + |T_{13} - 33.06| + \\ |T_{14} - 33.22| + |T_{15} - 32.75| + |T_{16} - 31.79| + \\ |T_{17} - 33.55| + |T_{18} - 34.75| + |T_{19} - 34.21| + \\ |T_{110} - 33.02| + |T_{21} - 29.24| + |T_{22} - 30.28| + \\ |T_{23} - 31.95| + |T_{24} - 34.02| + |T_{25} - 35.65| \end{aligned} \tag{4}$$

Here, $T_{1n}$ ($1 \le n \le 10$) and $T_{2m}$ ($1 \le m \le 5$), the temperature values of 15 equidistant points on two straight lines, were from the module "Objective Calculator". The calculation result $f_{min}$ was transmitted to the module "MIGA Optimization". The batch file was compiled and called into the module "ANSYS pork-fat 2-heatpoint". The parameter configuration used to execute the MIGA in this

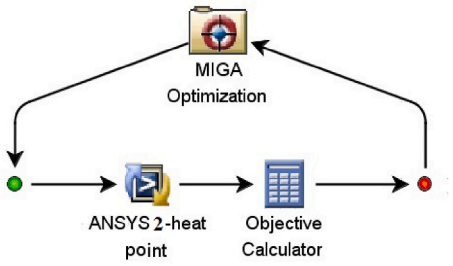


**Fig. 4.** ISIGHT flow diagram of reconstruction of heat sources in pork adipose tissue based on MIGA.

research is shown in Table 2.

After 250 generations and 10000 iterations, the optimal simulation position corresponding to the 30.5 Ω resistor heat source was (2.53 cm, 1.69 cm, 1.62 cm) and the one corresponding to the 15.5 Ω resistor heat source was (5.44 cm, 1.55 cm, 1.46 cm). The simulation temperature values corresponding to the two heat sources ware 85.92°Cand 61.55 °C, respectively. The detailed simulation images were shown as Fig. 5. Here, Fig. 5(a) was the surface temperature distribution diagram of cuboid adipose tissue in a whole field of view. Fig. 5(b) was the temperature distribution diagram of arbitrary section, which indicated one could acquire any interested temperature distribution section of adipose tissue module. Fig. 5(c) showed the temperature distribution of surface z = 3.0 cm, which was very approximate to the infrared thermal image of the same surface. Fig. 5(d), (e) and (f) were the temperature distribution sections that were parallel with the surfaces from three directions, and the corresponding sections were $z = 1.3$ cm, $x = 5.2$ cm and $y = 1.5$ cm respectively. These three sectional views could well incarnate the distribution characteristics of internal heat from different angles, and also reflect the status of internal heat sources.

## 5. Discussion and analysis

Comparing the experimental temperature values with the corresponding simulation ones, it is found that the simulation results acquired with MIGA are higher than those acquired with the infrared imager. The experimental and simulation temperature values of 15.5Ω resistor are 60.75°Cand 61.55 °C respectively, with the error of 3.9 %; The experimental and simulation temperature values of 30.5Ω resistor are 84.40 °C and 85.92°Crespectively, with the error of 3.5 %. As for the position of heat sources, the experimental and simulation position of 15.5Ω resistor are (5.6 cm, 1.5 cm, 1.4 cm) and (5.44 cm, 1.55 cm, 1.46 cm) respectively; and those of 30.5Ω resistor are (2.5 cm, 1.7 cm, 1.6 cm) and (2.53 cm, 1.69 cm, 1.62 cm) respectively. The comparing results show there is no significant difference between the positions measured in the experiment and those calculated in the simulation. The detailed comparison between the experimental and simulated values is shown in Table 3.

As is stated above in this present paper, this study has potential application prospects for tumor hyperthermia and disease thermal diagnosis technology, which is just the description from a methodological perspective. It does not mean that the temperature of the analyzed object must reach or exceed 80 °C to meet the use of the method proposed in this work. During tumor hyperthermia, the temperature of the lesion is raised to between 42.5–45 °C, which differs from the normal tissue temperature around. Therefore, the method proposed in this paper can be used to reconstruct the temperature field of the lesion and the tissue around.

From the perspectives of experimental model, experiment procedure and simulation model, the reasons of temperature error and position difference are analyzed as following: (1) The real biological tissue (pork adipose) is adopted in the experimental model, the thermophysical parameters of biological tissue will change correspondingly with the increase of its temperature. In the experiment procedure, the adipose tissue around the two resistors is melted in a small range, which is a main cause of temperature error of heat sources. It is seen from the results that the higher experimental temperature of heat sources will lead to the relatively significant error (When the experimental temperature is 60.75 °C, the error is 1.32 %, and when the experimental temperature is 84.40 °C, the error is 1.80 %). (2) In order to insert the resistors into the adipose tissue module, a narrow knife is used to make two incisions in different depths. There's still some heat coming out of the gap although the knife's width has been controlled to a reasonable scope. This is an another reason that causes errors. (3) The electrified wires can also create heat, which is equivalent of line heat sources set in the adipose tissue model. Compared with the heat created by the resistors, the heat created by the electrified wires is much smaller, but it is still an important factor that causes errors. (4) Because of the characteristics of biological soft tissue, the pork adipose model can be only controlled to be an approximate cuboid. But in the simulation process, the constructed model is set to be a standard 3D cubiod one. (5) The biological structures of pork adipose tissue is relatively complex, and the heat transfer in experiment model is anisotropic. In the simulation model, it is difficult to set the thermophysical parameters of adipose tissue to their true statethe, which is also an important reason leading to errors.

## 6. Conclusions

In this research, the real biological tissue is adopted in the experimental model. To investigate the noninvasive reconstruction of the internal heat source and the corresponding 3D temperature field, the MIGA algorithm and the large-scale finite element analysis software ANSYS are introduced in the simulation process, in which a suitable objective function is designed to fasten the iterative calculation. In the experiment part, two different resistors are used as the internal heat sources, and the related data acquired with the infrared imager are extracted for the computation and comparison in the objective function of optimization algorithm. In the simulation part, the APDL program is compiled to automatically perform the modeling, meshing, heat source setting, finite element calculation and temperature data acquiring of related nodes. It is shown from the results that the simulation distribution of surface temperature is consistent with the principle of heat transfer, and the simulation temperature values are slight above the experimental

**Table 2**
The parameter configuration adopted in MIGA.

| Parameter | $S_i$ | $S_t$ | $N_i$ | $N_g$ | $P_c$ | $P_m$ | $P_{mig}$ | $I_m$ |
|---|---|---|---|---|---|---|---|---|
| Set value | 10 | 40 | 4 | 250 | 0.8 | 0.02 | 0.1 | 5 |

**$S_i$**:Island size; **$S_t$**:Total scale of population; **$N_i$**:Number of islands; **$N_g$**:Number of generations.
**$P_c$**:Rate of crossover; **$P_m$**:Rate of mutation; **$P_{mig}$**: Rate of migration; **$I_m$**:Interval of migration.

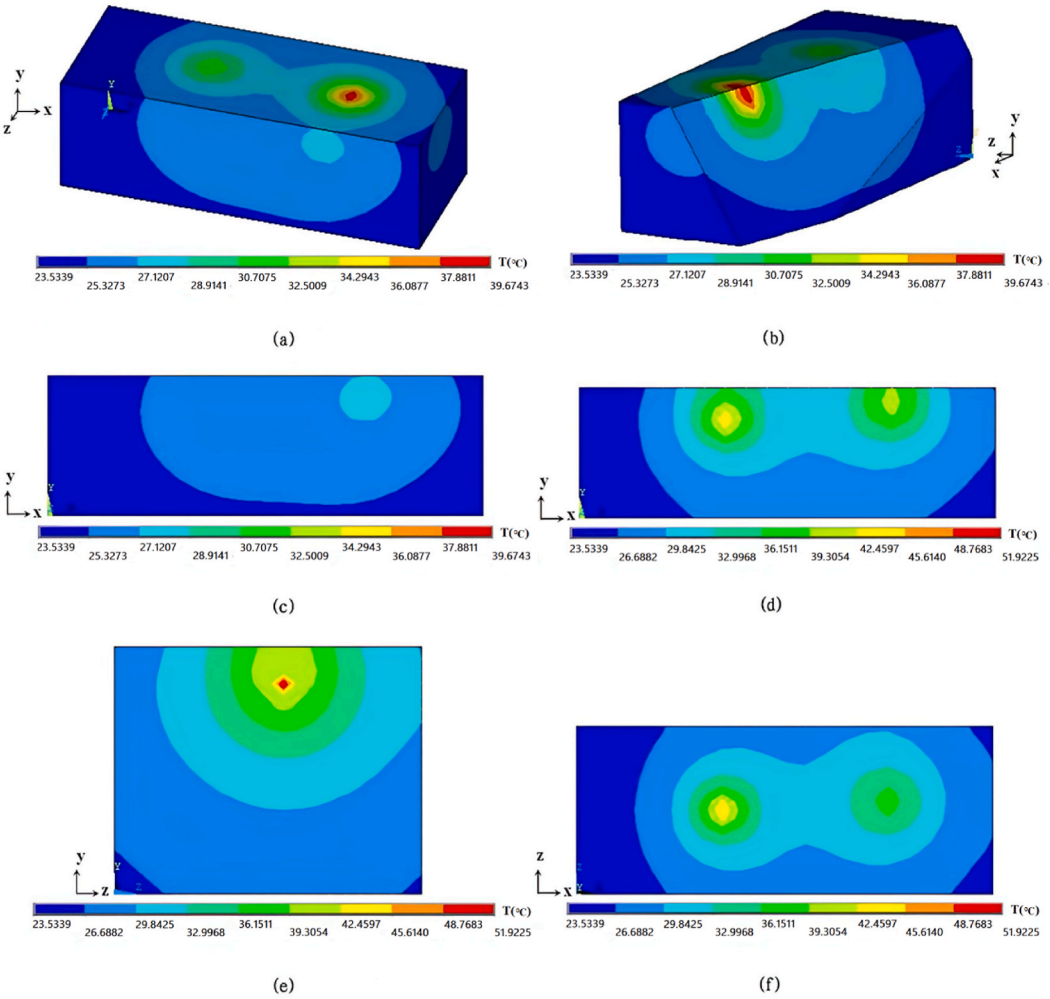


**Fig. 5.** Simulation results of 3D temperature field of pork adipose tissue based on MIGA.
(a) The full view of surface temperature distribution. (b) The temperature distribution of arbitrary section of adipose tissue module. (c) The temperature distribution of surface $z = 3.0$ cm. (d) The temperature distribution of section $z = 1.3$ cm. (e) The temperature distribution of section $x = 5.2$ cm. (f) The temperature distribution of section $y = 1.5$ cm.

**Table 3**
Comparison between experimental and simulated values.

| | Location of Resistor (30.5Ω) | | | Location of Resistor (15.5Ω) | | | Temperature of Resistor (30.5Ω)(°C) | Temperature of Resistor (15.5Ω)(°C) |
|---|---|---|---|---|---|---|---|---|
| | x (cm) | y (cm) | z (cm) | x (cm) | y (cm) | z (cm) | | |
| Simulation values | 2.53 | 1.69 | 1.62 | 5.44 | 1.55 | 1.46 | 85.92 | 61.55 |
| Measured values | 2.5 | 1.7 | 1.6 | 5.6 | 1.5 | 1.4 | 84.40 | 60.75 |
| Errors | | | | | | | 1.80 % | 1.32 % |

ones. In consideration of the environmental factors, measuring error factors and simulation parameter setting factors, the errors between the experiment results and simulation ones are within a reasonable range. This reconstruction method of 3D temperature field that combines the global optimization algorithm and the FEM is convenient and fast, and possesses broad application prospects in medical engineering field.

## Funding statement

This work is supported by the Medical Research Project of Hubei University of Science and Technology (Grant No.2023YKY09), the

Scientific Research Development Fund of Hubei University of Science and Technology (Grant No. 2019-21GP11), the China's Ministry of Education's Industry & University Collaborative Education Projects (Grant No. 230805160165452, 231107604030923, 230902116201223) and the Hubei Province College Students' Innovation and Entrepreneurship Training Project (Grant No. S202110927078S).

## Data availability statement

Data will be made available on request.

## Additional information

No additional information is available for this paper.

## CRediT authorship contribution statement

**Fuli Ye:** Writing – review & editing, Project administration, Methodology, Formal analysis, Conceptualization. **Diwen Shi:** Writing – original draft, Methodology, Investigation, Data curation. **Cheng Xu:** Software, Resources, Formal analysis. **Kaiyang Li:** Writing – review & editing, Methodology, Conceptualization. **Minyue Lin:** Methodology, Investigation, Funding acquisition, Data curation. **Guilian Shi:** Writing – review & editing, Supervision, Investigation, Funding acquisition, Data curation, Conceptualization.

## Declaration of competing interest

The authors declare no conflict of interest.

## Acknowledgments

We thank Hubei Sijie Medical Technology Co., Ltd. for providing a series of assistance in this study.

## References

[1] K. Das, S.C. Mishra, Estimation of tumor characteristics in a breast tissue with known skin surface temperature, J. Therm. Biol. 38 (6) (2013) 311–317, https://doi.org/10.1016/j.jtherbio.2013.04.001.
[2] D. Khan, A. Rahman, P. Kumam, Thermal analysis of different shape nanoparticles on hyperthermia therapy on breast cancer in a porous medium: a fractional model, Heliyon 8 (2022) e10170, https://doi.org/10.1016/j.heliyon.2022.e10170.
[3] M.G. Sobamowo, A.A. Yinusa, S.T. Aladenusi, Impacts of magnetic field and thermal radiation on squeezing flow and heat transfer of third grade nanofluid between two disks embedded in a porous medium, Heliyon 6 (2020) e03621, https://doi.org/10.1016/j.heliyon.2020.e03621.
[4] R. Shao, G. Zhang, X. Gong, Generalized robust training scheme using genetic algorithm for optical neural networks with imprecise components, Photonics Res 10 (8) (2022) 1868, https://doi.org/10.1364/PRJ.449570.
[5] Z. Li, Neural Network Economic Forecast Method Based on Genetic Algorithm, IET Software, 2023, https://doi.org/10.1049/sfw2.12090.
[6] D. Alves, D. Oliveira, E. Andrade, GPU-BRKGA: a GPU accelerated library for optimization using the biased random-key genetic algorithm, Lat. Am. T. (20–1) (2022), https://doi.org/10.1109/TLA.2022.9662169.
[7] M.I.M. Copetti, J.J.R. Durany, Numerical analysis and simulation of a bio-thermal model for the human foot, Appl. Math. Comput. 305 (2017) 103–116, https://doi.org/10.1016/j.amc.2017.01.067.
[8] A. Zingaro, I. Fumagalli, L. Dede, A geometric multiscale model for the numerical simulation of blood flow in the human left heart, Discrete Cont, Dyn. Syst. 15 (8) (2022) 2391–2427, https://doi.org/10.3934/dcdss.2022052.
[9] D. Luca, F. Menghini, A. Quarteroni, Computational fluid dynamics of blood flow in an idealized left human heart, Int. J. Numer. Meth. Bio. 31 (11) (2019) 1–24, https://doi.org/10.1002/cnm.3287, e3287.
[10] M.A. Alosaimi, D. Lesnic, Determination of the space-dependent blood perfusion coefficient in the thermal-wave model of bio-heat transfer, Eng. Computation. 40 (2) (2023) 411–433, https://doi.org/10.1108/EC-07-2022-0467.
[11] Z. Shomali, Robert Kovács, Peter Ván, et al., Recent progresses and future directions of lagging heat models in thermodynamics and bioheat transfer. https://doi.org/10.48550/arXiv.2103.00314, 2021.
[12] C. Yao, C. Chuang, A simple and efficient real-coded genetic algorithm for constrained optimization, Appl. Soft Comput. 38 (C) (2016) 87–105, https://doi.org/10.1016/j.asoc.2015.09.036.
[13] V.L. Tiwari, A. Thapar, R. Bansal, A Genetic algorithm for solving nonlinear optimization problem with max-archimedean bipolar fuzzy relation equations, Int. J. Uncertain. Fuzz. 31 (2023) 303–326, https://doi.org/10.1142/S0218488523500162.
[14] S.E. Chafi, Y. Balboul, M. Fattah, Enhancing resource allocation in edge and fog-cloud computing with genetic algorithm and particle swarm optimization, Intelligent and Converged Networks 4 (4) (2023) 273–279, https://doi.org/10.23919/ICN.2023.0022.
[15] E.J. Onyiriuka, O.O. Ighodaro, A.O. Adelaja, D.R.E. Ewim, S. Bhattacharyya, A numerical investigation of the heat transfer characteristics of water-based mango bark nanofluid flowing in a double-pipe heat exchanger, Heliyon 5 (2019) e02416, https://doi.org/10.1016/j.heliyon.2019.e02416.
[16] H.R. Kazemi, K. Khalili-Damghani, S. Sadi-Nezhad, Estimation of optimum thresholds for binary classification using genetic algorithm: an application to solve a credit scoring problem, Int. J. Knowl. Eng. 40 (3) (2023) e13203, https://doi.org/10.1111/exsy.13203, 1-27.
[17] G. Veerasamy, R. Kannan, R.K. Siddharthan, Integration of genetic algorithm tuned adaptive fading memory Kalman filter with model predictive controller for active fault-tolerant control of cement kiln under sensor faults with inaccurate noise covariance, Math. Comput. Simulat. 191 (2022) 256–277, https://doi.org/10.1016/j.matcom.2021.07.023.
[18] S. Sun, Y. Ji, Z. Chang, G. Wang, H. Chen, Reconstruction of surface laser power and internal temperature of biological tissue during laser-induced thermal therapy, Numer. Heat Transfer, Part A: Appl. 83 (5) (2023) 558–571, https://doi.org/10.1080/10407782.2022.2101803.
[19] S.C. Sun, Simultaneous reconstruction of thermal boundary condition and physical properties of participating medium, Int. J. Therm. Sci. 163 (2021) 106853, https://doi.org/10.1016/j.ijthermalsci.2021.106853.
[20] S. Sun, Z. Chang, Y. Ji, G. Wang, L. Wei, Inverse estimation of transient heat flux using sequential function specification method, Heat Transfer Eng 45 (3) (2024) 233–243, https://doi.org/10.1080/01457632.2023.2185488.

[21] S.C. Sun, Y.L. Ji, Z.H. Chang, G.J. Wang, L.Y. Wei, Application of stochastic particle swarm optimization algorization algorithm for noninvasive determination of temperature-dependent thermal properties of biological tissue, Heat Transfer Res 53 (11) (2022) 45–60, https://doi.org/10.1615/HeatTransRes.v53.i11.40.
[22] S. Sun, G. Wang, H. Chen, Application of improved decentralized fuzzy inference methods for estimating the thermal boundary condition of participating medium, Int. J. Therm. Sci. 149 (2020) 106216, https://doi.org/10.1016/j.ijthermalsci.2019.106216.
[23] B. San, Z. Xiao, Y. Qiu, Simultaneous shape and stacking sequence optimization of laminated composite free-form shells using multi-island genetic algorithm, Adv. Civ. Eng. 3 (2019) 1–14, https://doi.org/10.1155/2019/2056460.
[24] H. Kumar, B. Gupta, P. Singh, Genetic algorithm-based higher-order model reduction of proton exchange membrane fuel cell, Int. Fournal .Energy Res 19 (9) (2022) 1–14, https://doi.org/10.1002/er.8725.
[25] K. Boulanouar, A. Hadjali, M. Lagha, Trends summarization of times series: a multi-objective genetic algorithm-based model, J. Smart Environ. Green Comput. 2 (1) (2022) 19–33, https://doi.org/10.20517/jsegc.2021.25.
[26] F. Ma, L. Han, Y. Zhou, Multi-island genetic algorithm and Kriging model-based design of vehicle product comprising multi-material, IEEE Access 99 (2018), https://doi.org/10.1109/ACCESS.2018.2871776.
[27] J. Zhang, W. Liu, W. Liu, An efficient genetic algorithm for decentralized multi-project scheduling with resource transfers, J. Ind. Manag. Optim. 18 (1) (2022) 1–24, https://doi.org/10.3934/jimo.2020140.
[28] U. Yasmeen, M.A. Khan, U. Tariq, Citrus diseases recognition using deep improved genetic algorithm, Comput. Mater. Con. (2 Pt.3) (2022) 71, https://doi.org/10.32604/cmc.2022.022264.
[29] S.A. Ili, A. Selakov, S.M. Vukmirovi, Procedure for Creating Custom Multiple Linear Regression Based Short Term Load Forecasting Models by Using Genetic Algorithm Optimization, National Library of Serbia, 2021, https://doi.org/10.2298/TSCI1912051011.
[30] R. Hans, H. Kaur, Hybrid biogeography-based optimization and genetic algorithm for feature selection in mammographic breast density classification, Int. J. Image Graph. (2021) 2140007, https://doi.org/10.1142/S0219467821400076.
[31] F. Marchi, R.S. Parpinelli, A Multi-objective approach to the protein structure prediction problem using the biased random-key genetic algorithm, in: IEEE Congress on Evolutionary Computation (CEC), 2021, pp. 1071–1077, https://doi.org/10.1109/CEC45853.2021.9504745.
[32] B. Arasteh, M.J. Hosseini, An error-propagation aware method to reduce the software mutation cost using genetic algorithm, Data Technol. Appl. 1 (2020) 118–148, https://doi.org/10.1108/DTA-03-2020-0073.
[33] H. Diao, Deep Mining of redundant data in wireless sensor network based on genetic algorithm, Autom. Control Comput. 52 (4) (2018) 291–296, https://doi.org/10.3103/s0146411618040053.
[34] Hossain Delowar, Genci, et al., Optimizing deep learning parameters using genetic algorithm for object recognition and robot grasping, J. Electron. Sci. 16 (1) (2018) 11–15, doi:CNKI:SUN:ZGKE.0.2018-01-002.
[35] L. Yin, J. Qiu, S. Gao, Biclustering of gene expression data using cuckoo search and genetic algorithm, Int. J. Pattern Recogn 32 (11) (2018) 1850039.1–185003931, https://doi.org/10.1142/S0218001418500398.
[36] C. Xuerui, Three-dimensional image art design based on dynamic image detection and genetic algorithm, J. Intel. Fuzzy Syst. 5 (2020) 1–12, https://doi.org/10.3233/JIFS-189567.
[37] Montri, B. Veera, I. Sarun, Artificial neural network and genetic algorithm hybrid intelligence for predicting Thai stock price index trend, Comput. Intel. Neurosc. (2016) 1–8, https://doi.org/10.1155/2016/3045254.
[38] Z. Wang, J. Ma, L. Zhang, State-of-health estimation for lithium-ion batteries based on the multi-island genetic algorithm and the Gaussian process regression, IEEE Access 5 (2017) 1, https://doi.org/10.1109/ACCESS.2017.2759094.
[39] P. Ren, S. Meng, W. Yi, Scheduling technology of satellites parallel final assembly based on Multi-island Genetic Algorithm, J. Phys. Conf. 1650 (2020) 032201, https://doi.org/10.1088/1742-6596/1650/3/032201.
[40] J. Cheng, H. Li, B. Fu, Optimization of metal belt continuously variable transmission pulley based on multi-island genetic algorithm, in: Microelectronics Systems Education, IOP Publishing, 2019, https://doi.org/10.1088/1757-899x/612/3/032198.
[41] P. Zhang, H.X. Wang, X.D. Zhang, Structural parameter optimization design of torsion beam semi-independent suspension based on multi-island genetic algorithm, Appl. Mech. Mater. 893 (2019) 109–115, https://doi.org/10.4028/www.scientific.net/AMM.893.109.
[42] H.H. Pennes, Analysis of tissue and arterial blood temperature in the resting human forearm, J. Appl. Physiol. 1 (1948) 93–122.
[43] J. Luo, D.E. Baz, A dual heterogeneous island genetic algorithm for solving large size flexible flow shop scheduling problems on hybrid multi-core CPU and GPU platforms, Math. Probl Eng. 2 (2019) 1–13, https://doi.org/10.1155/2019/1713636.
[44] Q. Zhang, Y. Luo, W. Lin, Control and optimisation of a dual-motor coupling drive system of pure electric vehicle based on multi-island genetic algorithm, Int. J. Electr. Hybrid 13 (1) (2021), https://doi.org/10.1504/IJEHV.2021.115195.
[45] W. Wang, S. Yuan, J. Pei, Optimization of the diffuser in a centrifugal pump by combining response surface method with multi-island genetic algorithm, P. I. Mech. Eng. E- J. Pro. 231 (2) (2017) 191–201, https://doi.org/10.1177/0954408915586310.
[46] Z. Dong, D. Liu, C. Liang, Optimization of film cooling arrays on a gas turbine vane by using an integrated approach of numerical simulation and parameterized design, Appl. Therm. Eng. 81 (2022) 304–313, https://doi.org/10.1016/j.applthermaleng.2022.119464.